Journal of Power Sources 210 (2012) 233–242

Contents lists available at SciVerse ScienceDirect

Journal of Power Sources

journal homepage: www.elsevier.com/locate/jpowsour

A damage model for degradation in the electrodes of solid oxide fuel cells: Modeling the effects of sulfur and antimony in the anode

E.M. Ryan [a,*], W. Xu [b], X. Sun [b], M.A. Khaleel [b]

[a] Boston University, Department of Mechanical Engineering, 110 Cummington Street, Boston, MA 02215, USA
[b] Pacific Northwest National Laboratory, Computational Sciences and Mathematics Division, P.O. Box 999, Richland, WA 99352, USA

ARTICLE INFO

Article history:
Received 15 November 2011
Received in revised form 22 February 2012
Accepted 23 February 2012
Available online 29 March 2012

Keywords:
Solid oxide fuel cell
Degradation
Computational model
Sulfur poisoning
Antimony
Damage factor

ABSTRACT

Over their designed lifetime, high-temperature electrochemical devices, such as solid oxide fuel cells (SOFCs), can experience degradation in their electrochemical performance due to environmental conditions, operating conditions, contaminants, and other factors. Understanding the different degradation mechanisms in SOFCs and other electrochemical devices is essential to reducing performance degradation and increasing the lifetimes of these devices. In this paper, SOFC degradation mechanisms are evaluated, and a damage model is presented that describes performance degradation in SOFCs due to damage or degradation in the SOFC electrodes. A degradation classification scheme is presented, dividing the various SOFC electrode degradation mechanisms into categories based on their physical effects on the SOFC. The damage model and classification method are applied both to sulfur poisoning and antimony poisoning, which occur in the SOFC anode. For sulfur poisoning, the model can calculate degradation in SOFC performance based on the operating temperature of the fuel cell and the concentration of gaseous sulfur species in the anode. For antimony poisoning, the effects of nickel consumption from the anode matrix are investigated.

1. Introduction

Solid oxide fuel cells (SOFCs) and other electrochemical devices, such as proton exchange membrane (PEM) fuel cells and batteries, are promising alternative energy devices that are being considered for applications ranging from full-scale power generation to small-scale portable power systems. SOFCs are being developed for stationary and auxiliary power applications, which require a 40,000 h or more lifetime [1]. The power output and long-term performance and degradation of electrochemical devices rely heavily on the reactive transport and electrochemical performance within the electrodes. In SOFCs, performance degradation can be caused by a number of factors, including environmental and operating conditions, contaminants in the fuel and air streams, and impurities in materials and balance of plant equipment. These various degradation mechanisms can rapidly reduce the power output of SOFCs, as in the case of sulfur poisoning [2,3], or gradually affect performance over the SOFC's operating lifetime, as with chromium poisoning [4].

To improve the performance and lifetime of electrochemical devices, it is important to understand the various degradation mechanisms that occur within the electrodes and how they are affected by the local conditions within the electrodes. Experimental studies of degradation mechanisms focus on the effects to overall performance without resolving the physics within the electrodes and electrolyte of a working fuel cell [2,5]. In SOFCs, the high operating temperatures and complex, compact geometry make it difficult for experimentalists to get detailed data on the conditions within the fuel cell. Computational modeling is able to simulate the multi-physics reactions occurring within the electrodes and investigate the local physical mechanisms that cause the degradation in overall SOFC performance.

Herein, we present a degradation modeling framework for SOFCs. The degradation modeling framework is intended to be general and can be used to consider various degradation mechanisms in SOFCs and other electrochemical devices. As part of the framework, a classification system for the different degradation mechanisms is developed, which classifies the mechanisms based on their effects on the SOFC (such as structural or chemical changes), and is used to establish degradation models based on continuum damage mechanics [6]. The continuum damage approach accounts for degradation in the SOFC electrodes through a damage factor, which is applied (as appropriate) to model parameters such as transport properties, porosity, or triple phase boundary (TPB) length. The model is applied to the distributed electrochemistry (DEC) model, which simulates the multi-physics through the thickness of the electrodes and electrolyte [7].

* Corresponding author. Tel.: +1 617 353 7767; fax: +1 617 353 5866.
E-mail address: ryanem@bu.edu (E.M. Ryan).

0378-7753/$ – see front matter © 2012 Elsevier B.V. All rights reserved.
doi:10.1016/j.jpowsour.2012.02.091

Table 1
Effects of trace species in gasified coal on the SOFC anode [5,14,19,20].

Species	Observed reactions	Effect on SOFC	Trends with SOFC operation
Phosphorus (P)	Adsorbs to anode, forms Ni_xP_y on surface	Gradual increase of ohmic and electrodic polarization; sharp performance drop at high P concentration and formation of microcracks. Loss of electrical percolation. Poisoning occurs from the fuel channel and propagates into anode	Rates of degradation show no significant dependence on current density or fuel utilization. Increases with P concentration
Arsenic (As)	Ni consumption and migration from the anode matrix	Abrupt failure after long-term operation due to loss of electrical percolation	Depth of reaction area and agglomeration increase with AsH_3 concentration; no significant dependence on current density or fuel utilization
Selenium (Se)	Adsorbs near electrolyte interface; nanoparticles form at medium and high polarization; forms Ni_xSe_y at high current density	Rapid decrease in power to new steady state. Primarily an increase in electrodic polarization; minimal increase in ohmic loss; at intermediate current oscillatory behavior. Possible Ni_xSe_y at interface due to increase in O_2 partial pressure (p_{O_2}). Partially reversible at low current	Increases with current and Se concentration; oscillations in performance at intermediate current; local p_{O_2} increases with large current
Sulfur (S)	Adsorbs to anode; may form Ni_xS_y at high current density	Rapid decrease in power to new steady state. At high current density Ni redistribution to small particles at electrolyte interface. Partially reversible under certain conditions	Increases with decreasing operating temperature; increases with increasing S concentration; increases with increasing operating voltage
Chlorine (Cl)	Adsorption of Cl to the Ni surface and possible sublimation of $NiCl_2$	Reversible increase in electrodic polarization, decrease in ohmic loss at 700 °C due to scavenging effect of HCl	Higher HCl concentration leads to faster voltage change; degradation rate does not show dependence with polarization
Antimony (Sb)	Adsorption of Sb and formation of Ni_xSb_y on surface; Ni consumption and migration from matrix	Two-stage degradation: initial rapid decrease in voltage with increase in electrodic polarization; longer-term decrease in voltage with increase in ohmic loss. Loss of electrical percolation due to Ni_xSb_y	Initial stage: Nearly independent of Sb concentration; increasing degradation with decreasing current density. Late stage: Ni–Sb crystallite size grows with Sb

This paper is divided into five sections. Section 1 provides a general overview of degradation mechanisms in SOFC electrodes. Section 2 discusses the classification of these degradation mechanisms based on their effects on the electrodes. In Section 3, the degradation model is outlined, and the application of the degradation model to sulfur and antimony poisoning are presented in Section 4. The final section discusses the conclusions drawn from this work and future direction of this research.

2. Degradation mechanisms in SOFC electrodes

Degradation within the SOFC electrodes can lead to dramatic decreases in overall performance. Degradation occurs due to a number of factors, including operating conditions [8], mismatch of material properties, the presence of trace species in materials and balance of plant equipment [9], or the presence of contaminant species in the gas streams [5]. SOFCs operate under extreme temperatures and electrochemical conditions that can lead to interactions between materials and induce stress due to mismatched material properties, such as the coefficient of thermal expansion (CTE) [10,11]. Operating conditions, such as temperature, voltage, and fuel utilization, also can lead to degradation issues, including the formation of coke in the anode [8]. Contaminants in the SOFC's fuel and air streams can cause a variety of degradation issues, especially in the anode. Due to their high operating temperature, SOFCs are fuel flexible and are being considered for use with gasified coal, biofuels, and other alternative fuel sources. The trace species found in these alternative fuel sources can interact with the anode material and decrease the SOFC's electrochemical performance.

In particular, gasified coal contains numerous trace species that can interact with the SOFC anode [12]. Depending on where the coal is mined and how it is processed, the concentrations and specific trace species can vary significantly. The SOFC anode, typically a mixed conducting composite electrode consisting of nickel (Ni) and yttria-stabilized zirconia (YSZ), is known to react with many of these species. The responses of the anode and SOFC performance to trace species can vary from a decrease in performance to a lower steady-state performance, as seen with sulfur poisoning, to an abrupt failure of the cell, such as with arsenic [5]. Several experimental studies have investigated the various trace species found in gasified coal and their effects on the SOFC anode [2,5,13–18]. An overview of coal gas contaminant species that affect the SOFC is shown in Table 1. As seen in the table, the different trace species affect different aspects of the anode's performance, such as the percolation of the electron-conducting material through the anode thickness, the availability of Ni for electrochemical reactions, and the porosity of the anode.

The diversity of degradation mechanisms in the SOFC electrodes leads to a variety of physical changes to the SOFC microstructure and chemical properties, which affect the SOFC's overall performance. Simulating these degradation mechanisms requires the development of a unique model for each case. In the following sections, we discuss a flexible modeling framework that aids the classification of different degradation mechanisms and development of the various models.

Table 2
Continuum-scale model parameters.

Symbol	Variable
ε	Porosity
τ	Tortuosity
κ	Permeability
r_p	Pore radii
r_g	Grain radii
λ	Thermal conductivity
σ	Ionic (ion) or electrical (e^-) conductivity
D_{surf}	Surface diffusion
TPB	Triple phase boundary length
K_{react}	Reaction rate
K_{CT}	Charge transfer reaction rate
f_{vol}	Volume fraction

3. Classifying degradation

To facilitate the modeling and investigation of the different degradation mechanisms that occur in SOFCs, we can classify the various mechanisms based on their effect on the SOFC's electrodes and how they relate to different parameters of a continuum scale model (Table 2), e.g. the DEC model [7]. Fig. 1 flow chart classifies degradation by addressing the question of how different contaminants and degradation mechanisms affect the SOFC electrodes. In all degradation cases, the overall effect on the SOFC electrodes is a change in the rate of electrochemical reactions within the electrode. Depending on the specific degradation case, this effect can take many forms. In the case of sulfur poisoning, sulfur adsorbs to the anode surface and blocks the electrochemical reaction sites. In the case of CTE mismatch, cracking and delamination of the electrodes can occur, damaging the physical microstructure and disrupting the flow of ions and electrons in the solid to the TPB sites.

Our classification scheme divides the effects of degradation into two broad categories: (1) structural and (2) chemical effects. Structural effects change the physical structure of the SOFC, while chemical effects involve the composition and chemical (or electrochemical) reactions in the SOFC. The structural category is further divided into subcategories based on how the degradation is affecting the microstructure:

- Flow blockage occurs when the pore space of the electrodes becomes obstructed, such as with the formation of a precipitate. Flow blockage will typically affect the porosity (ε), tortuosity (τ), permeability (κ), and pore radii (r_p) of the electrode.
- Delamination happens when different layers of the SOFC come apart, such as at the interface of the electrode and electrolyte. With delamination, the percolation of the ionic- and electronic-conducting phases will be interrupted, decreasing the electrode's conductivity (σ). Delamination also will affect the basic porous microstructure, as well as the ε, τ, κ, and r_p parameters.
- Particle formation/coarsening occurs when one of the components of the electrode changes in volume due to the formation of a new phase. Ni coarsening in the anode [21,22] is an example of this category.
- Structural collapse or instability includes the formation of cracks in the microstructure or failure of the microstructure because of a loss of structural integrity [5,19]. This can occur due to the migration of material from the electrode, a non-uniform change in the electrode's volume, or other structural changes in the electrodes.

In the chemical effects category, there are also several subcategories that describe the various ways degradation mechanisms interact chemically with the electrodes:

- Adsorption of contaminant species is a common degradation issue [23], which decreases the reactive surface area (TPB length) and surface diffusion of the electrode and can affect the reaction rates in the electrode.
- Migration of species from the electrode composite microstructures occurs with a number of coal contaminants, such as Sb, in which Sb reacts with Ni and forms Ni_xSb_y near the anode surface (Fig. 2) [20], or phosphorus (P), which forms Ni_xP_y and disrupts the percolation of the electrode [19]. In both case Ni migrates from the Ni–YSZ matrix to form secondary phases which affect the electrochemical performance of the cell. As in the case of Ni_xSb_y and Ni_xP_y, many times the secondary phase is seen to migrate to the anode surface.
- Composition changes occur in the electrodes when the components of the microstructure react with a contaminant to form a new material, such as in chromium poisoning where chromium reacts with magnesium in the cathode to form spinel crystals ($(Cr,Mn)_3O_4$) [24].
- Electrochemical reactions of contaminant species with the electrodes block the electrodes' TPB sites and reduce the electrons available for the main electrochemistry of the SOFC.

The classifications shown in Fig. 1 along with the modeling parameters they affect can be used to develop models of the various degradation mechanisms occurring in the SOFC electrodes. Classifying the various contaminants and degradation mechanisms by their effects on the SOFC electrodes highlights the modeling parameters influenced by the degradation mechanism and allows similarities between degradation mechanisms to be easily identified. The categorization shown in Fig. 1 is based on the available data on degradation in SOFCs. However, it is not meant to be an exhaustive classification. As new data becomes available and new issues arise in SOFCs this classification framework can be expanded to include new degradation mechanisms and new theories on existing degradation mechanisms. The categories shown here are meant to guide the development of computational models and to lay out a framework for thinking about degradation. Additionally, degradation mechanisms, such as those in Table 1, can fall into more than one of the categories outlined in Fig. 1. For instance, phosphorus poisoning occurs when P reacts with Ni to form Ni_yP_x (composition), which causes an increase in volume of the Ni particles (particle forming/coarsening), leading then to the formation of microcracks (instability/collapse) [19].

4. Degradation modeling

Based on the categorization of the various degradation mechanisms in the SOFC electrodes, degradation models can be developed to investigate the effects of degradation on the electrodes and of operating and local conditions on the rates and magnitude of degradation. Modeling degradation can take place at a number of scales – from fundamental models investigating the reactions and transport at the surfaces and interfaces of the electrodes [25–27] to large-scale, stack-level modeling [28] that considers the effects of degradation on overall system performance. We focus on cell-level models with the objective of resolving degradation within the SOFC electrodes and having the ability to calculate the effects of local degradation in the electrodes on the performance of a single SOFC. We propose a continuum damage approach [6] for modeling degradation in the electrodes. In the continuum damage approach, a damage factor is used to simulate the effects of structural damage. In our degradation modeling, a damage factor (f) is used to modify properties and model parameters of the electrodes, such as those listed in Table 2 to account for the effects of a specific degradation mechanism on the SOFC electrode.

Based on the categorization of the various degradation mechanisms (Section 2), we can model the effects of a specific degradation

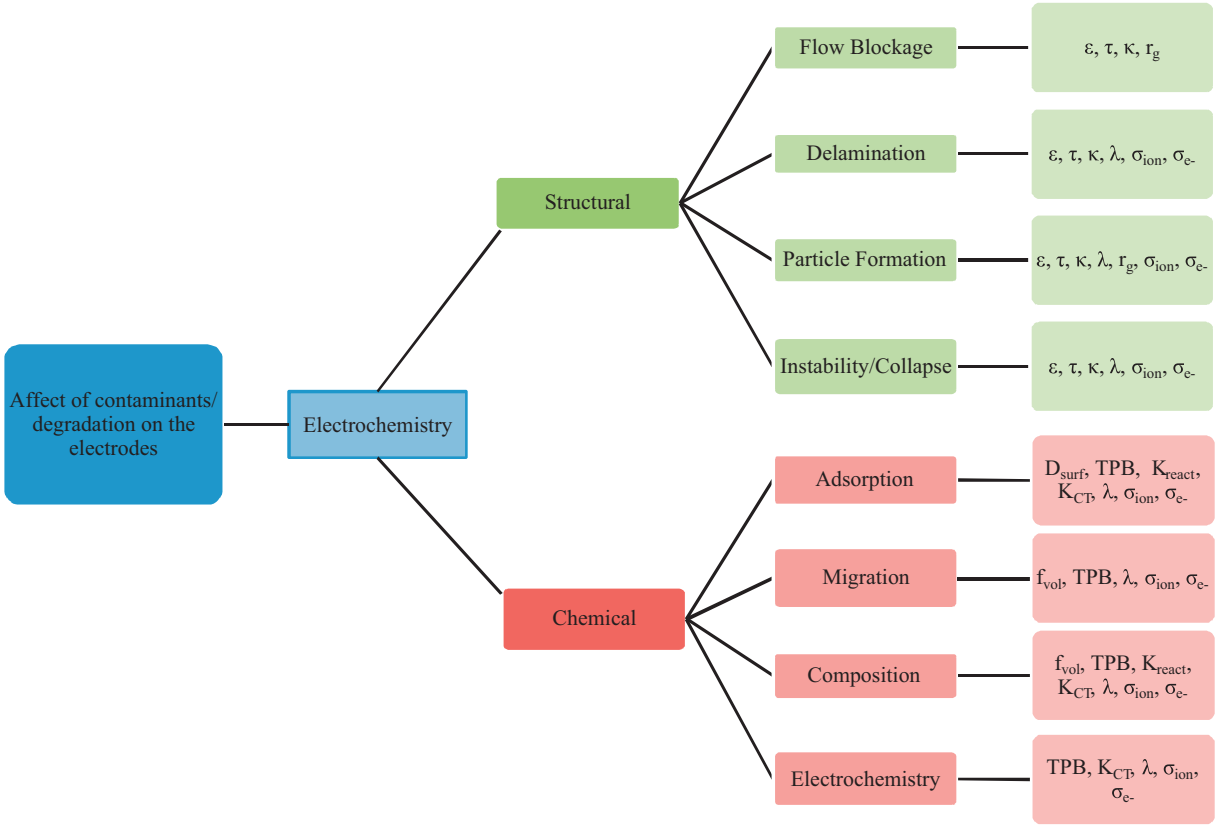

Fig. 1. Classification flow chart for degradation in the electrodes of an SOFC. Symbols are defined in the text and in Table 2.

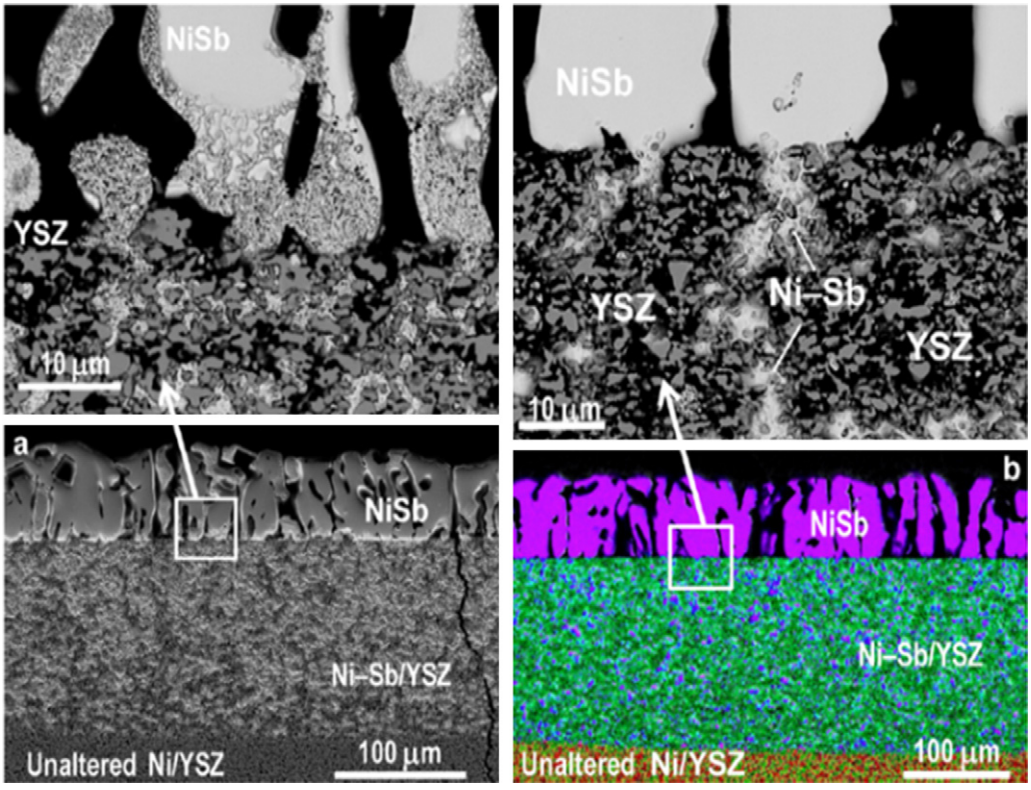

Fig. 2. SEM images and X-ray elemental color map of the effects of antimony on the upper region of an SOFC anode. Reprinted from Marina et al. [20], with permission from Elsevier.

mechanism by modifying model parameters associated with that mechanism, as listed in Fig. 1 and Table 2. For example, if a contaminant species reacted with the SOFC cathode to form a precipitate (flow blockage), it would cause a decrease in the cathode's porosity. Using a damage factor, this phenomenon could be quantified as:

$$\varepsilon^* = \varepsilon \times (1 - f), \tag{1}$$

where ε is the initial porosity of the cathode before degradation, ε^* is the porosity after the precipitation has occurred, and f is the damage factor with $0 \le f \le 1$. The initial porosity is decreased based on the damage factor. Depending on the degradation mechanism of interest, f can be constant or a function of space, time, species concentrations, etc. The form of f will depend on the degradation mechanism of interest and can be determined from experimental data and/or detailed small-scale models.

The use of the damage factor affords a flexible modeling framework that can be used to consider various degradation mechanisms and allows the degradation model to be easily coupled with different models. Two examples of degradation modeling in the SOFC anode will be discussed in Section 4. Both cases consider the effects of a coal gas contaminant (Table 1) on the performance and properties of the anode using a damage factor model coupled with an electrode or cell level model.

5. Degradation case studies

5.1. Sulfur poisoning in an SOFC anode

Sulfur poisoning occurs when hydrogen sulfide (H_2S) enters the SOFC anode with the fuel gas flow. H_2S is a trace species often found in gasified coal mixtures, and the amount of sulfur can vary significantly depending on the source of the coal and gasification process [5,12,17]. For example coal from Ohio and Pennsylvania typically contain 3%–10% sulfur by weight, while coal from Wyoming typically has less than 1% sulfur by weight [29]. To investigate the effects of sulfur poisoning on SOFC performance, a degradation model was developed based on applying a damage factor to the TPB length in the anode. H_2S has been shown to adsorb to the surfaces of the anode and block H_2 adsorption [23,30]. This reduces the surface area available for the electrochemical reactions in the anode, causing a reduction in the SOFC's overall performance. In SOFC modeling, the surface area available for electrochemical reactions is represented by the TPB length. As seen in Fig. 1, an adsorption degradation mechanism also could affect other parameters, such as surface diffusion and reaction rates. Based on conversations with experimentalists [23], we concluded that TPB length was the most appropriate parameter to reflect degradation due to sulfur poisoning.

Based on the experimental data of Zha et al. [3], we developed a functional form for the damage factor, which is a function of the local gas concentration of H_2S (c_{H_2S}) and temperature (T) in the anode. The damage factor is applied to the TPB length as:

$$l^*_{TPB} = l_{TPB} \times (1 - f(T, c_{H_2S})), \tag{2}$$

where l^*_{TPB} is the damaged TPB length and l_{TPB} is the initial TPB length before the introduction of H_2S to the gas stream. Zha et al. [3] performed button cell experiments on sulfur poisoning at 973 K, 1073 K, and 1173 K at a constant voltage of 0.7 V. At each temperature, experiments were run at seven different concentrations of H_2S in the fuel stream (0.2, 1, 2, 4, 6, 8, and 10 ppm H_2S ppm^{-1} H_2). The fuel mixture consisted of 50% H_2, 48.5% N_2, and 1.5% H_2O.

The continuum-scale DEC model [7] was used to simulate the SOFC's performance. The DEC model simulates the multi-physics of the SOFC, including the electrochemistry, through the thickness of the electrodes and electrolyte. In the DEC model, the electrochemistry takes place throughout the electrodes and is calculated using a modified Butler–Volmer relation [31], which calculates a local Faradaic current density based on the local gas concentrations. To determine the SOFC's global current density, the local Faradaic current density is integrated over the thickness of the electrodes. The modified Butler–Volmer relation includes the TPB length of the electrode as a parameter. The properties of the electrodes, such as the TPB length, are allowed to vary spatially in the DEC model. This feature was used to model the damage factor locally within the anode based on the local concentration of H_2S.

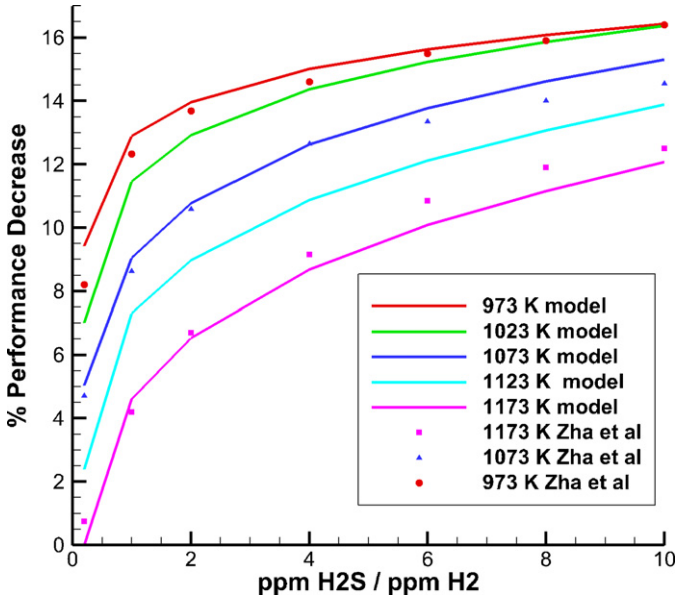

Fig. 3. Plot of the percent of SOFC performance decrease due to sulfur poisoning. The lines represent the results of the degradation model, while the symbols are the experimental data from Zha et al. [3].

A two-dimensional (2-D), axi-symmetric button cell geometry based on the experimental setup of [32] was modeled using the DEC model with a baseline (no H_2S) fuel composition of 50% H_2, 48.5% N_2, and 1.5% H_2O. H_2S was introduced to the button cell with the flue gas at the concentrations used by Zha et al. [3]. H_2S was allowed to diffuse through the anode with the gas mixture, and the local H_2S concentrations were used to calculate the local damaged TPB length:

$$l^*_{TPB}(\vec{x}) = l_{TPB}(\vec{x}) \times (1 - f(T, c_{H_2S}(\vec{x}))). \tag{3}$$

To determine a functional form of f, the degradation model was fit to the data from Zha et al. [3] at 1073 K:

$$f(T, c_{H_2S}(\vec{x})) = \alpha(T) \ln(c_{H_2S}(\vec{x})) + \beta(T), \tag{4}$$

where $\alpha(T)$ and $\beta(T)$ are:

$$\alpha(T) = 3.01 \times 10^{-22} T^{6.71} \tag{5}$$

$$\beta(T) = -2.25 \times 10^{-4} T + 0.7164. \tag{6}$$

Incorporating the functional form of f, the DEC model was used to simulate the change in performance due to sulfur poisoning over the temperatures and concentrations of H_2S considered by Zha et al. [3], as well as the same concentrations at 1023 K and 1123 K. The change in performance was calculated as [33]:

$$P = \frac{i_o - i}{i_o}, \tag{7}$$

where i_o is the baseline current density of the cell (no H_2S) and i is the damaged current density of the cell.

Fig. 3 shows the performance decrease due to sulfur poisoning predicted by the degradation model (solid lines) and experimental

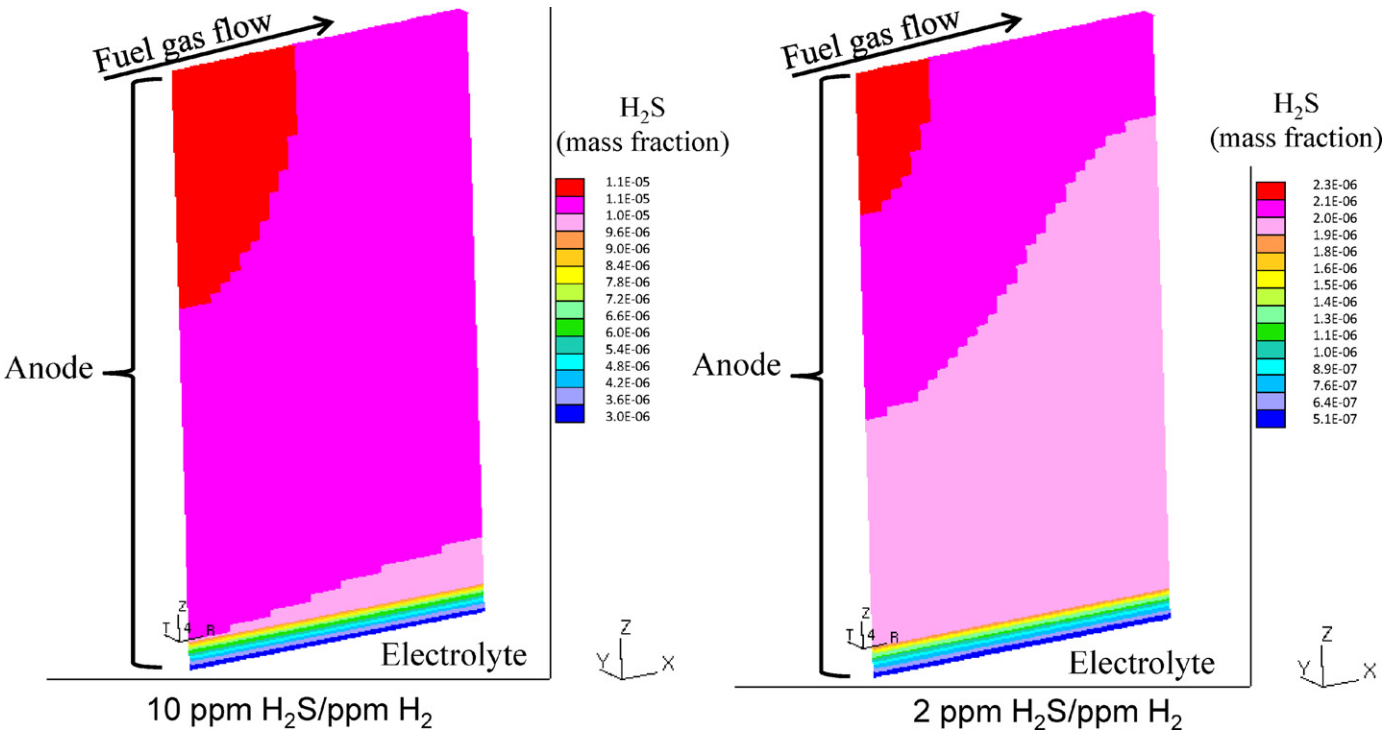

Fig. 4. Mass fraction of H_2S in the anode for 10 ppm H_2S ppm^{-1} H_2 (left) and 2 ppm H_2S ppm^{-1} H_2 (right) at 1073 K. H_2S enters the anode with the fuel from left to right along the top of the anode. Note the order of magnitude difference in mass fraction of H_2S between the two cases.

data (symbols) reported by Zha et al. [3]. The constants in α and β (Eqs. (5) and (6)) are fit to the experimental data of Zha et al. [3] at 1073 K. Those constants are then used to model the same system at 973 K and 1173 K and are compared to the experimental data. The degradation model is able to predict the performance decrease at 973 K and 1173 K with an average relative difference of 3.6%.

Using the DEC model allows us to resolve the local conditions within the electrodes, such as the H_2S concentration shown in Fig. 4 for the cases at 1073 K and with 10 and 2 ppm H_2S ppm^{-1} H_2. As shown in Fig. 4, the mass fraction of H_2S varies significantly through the thickness of the anode, which will lead to different levels of damage to the TPB length. Also, the mass fraction of H_2S of the 10 ppm H_2S ppm^{-1} H_2 differs from that of the 2 ppm H_2S ppm^{-1} H_2 by almost an order of magnitude, resulting in a roughly 4% difference in performance drop (Fig. 3).

Sulfur poisoning in the anode also depends on the operating voltage [3] and steam to carbon ratio (SC) [34] of the SOFC. Inclusion of these effects in the damage model, Eq. (3), would increase the applicability of the model and allow for a more detailed study of sulfur poisoning. Without including the effects of voltage and SC the current model is limited to cases with the operating conditions and fuel compositions presented in Zha et al. [3]. Future research on sulfur poisoning will endeavor to include the effects of voltage and SC to provide a more versatile modeling tool.

5.2. Antimony in an SOFC anode

In this section, we demonstrate another anode degradation case with antimony, which exists in coal mainly as oxides (Sb_xO_y) and sulfides (Sb_2S_3). The Sb content in U.S. coals averages 1.2 ppm [35]. However, higher concentrations, up to 3800 ppm, have been found in specific coal deposits [36]. When gasified coal is used as a fuel in SOFCs, volatized Sb will strongly interact with the Ni-YSZ anode. After an initial stage of a reversible antimony diffusion/adsorption-driven poisoning, prolonged exposure to Sb results in extensive formation of nickel antimonide compounds (such as NiSb and Ni_5Sb_2) inside the anode, which coalesces and eventually reduces the electrical percolation of the anode, leading to an abrupt performance loss in SOFCs [20]. Because YSZ is an electrical insulator, the Ni evolution alone is responsible for changes in the electrical conduction path. The percolation loss can then be described as Ni depletion. Removing Ni reduces the electrical conductive paths (electrical percolation) available between particles and causes a reduction in the effective electrical conductivity of the anode, leading to the SOFC's performance degradation. Here, it should be noted that the removal of Ni is used to model the local electrical conduction loss due to the Ni consummation through the reaction with contaminant materials or Ni migration.

In SOFC modeling, the electrical percolation can be represented by the volume fraction of Ni (V_{Ni}). A damage factor (f) can be applied to V_{Ni} to account for Sb poisoning as:

$$V_{Ni}^{*} = V_{Ni} \times (1 - f), \tag{8}$$

where V_{Ni}^{*} is the Ni volume fraction of the damaged (poisoned) anode.

To model the effects of Sb on V_{Ni}, a microstructure-based finite element (FE) model of the Ni–YSZ anode was developed. For computational convenience, a representative volume element (RVE) was modeled instead of the entire anode structure. The scanning electron microscope (SEM) image of the Ni–YSZ microstructure [19] (shown in Fig. 5a) is the RVE representing a cross section of the Ni–YSZ anode. It is a rectangular section with a thickness (D_o) of 30 μm and width (L_o) of 42 μm. Mixed elemental mapping of the SEM image analyzed using ImageJ gives the initial area fractions of Ni (red), zirconia (blue), and pores (black) within the microstructure. A 2-D triangular mesh was created with the grid generation software package, Gridgen (shown in Fig. 4b), and exported into ABAQUS for FE modeling and analysis. A thermal electrical analysis was conducted on the RVE with 31,700 coupled thermal–electrical linear triangular elements and 17,446 nodes.

Because the size of Ni–Sb crystallites increase with Sb concentration and exposure time [20], we propose a functional form for

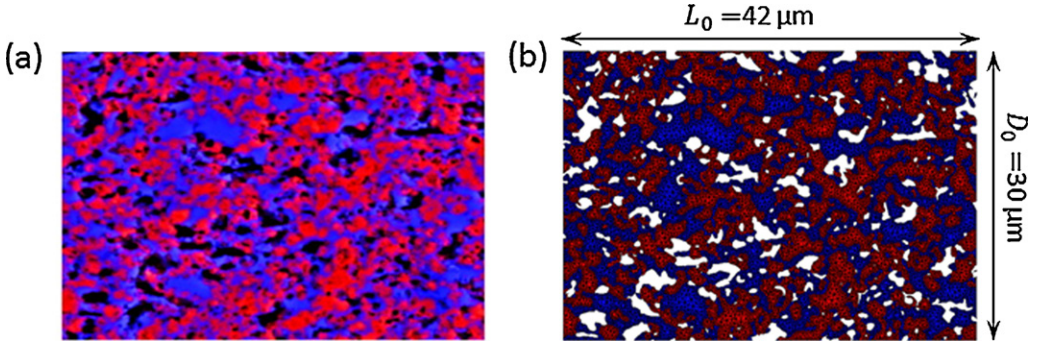

Fig. 5. (a) Ni–YSZ microstructure and distribution of the phases and (b) the FE model of the anode RVE. Nickel is shown in red, YSZ in blue, and the pores in black (shown white in (b)). (For interpretation of the references to colour in this figure legend, the reader is referred to the web version of this article.)

the damage factor as $f(c_{Sb}(x,t))$ to compute the overall electrical percolation loss of the anode. Here, $c_{Sb}(x,t)$ is the transient local Sb concentration, and $x = D/D_0$ represents the normalized depth. D denotes the depth from the anode top surface (at the fuel channel) where Sb starts to penetrate, and D_0 is the overall thickness of the RVE. We can then write Eq. (8) as:

$$V^*_{Ni}(x) = V_{Ni}(x) \times (1 - f(c_{Sb}(x,t))). \tag{9}$$

Assuming a Heaviside functional form for $c_{Sb}(x,t)$ as:

$$c_{Sb}(x,t) = c_{Sb}(x) \times \int_0^t \delta(t - t_p(x))dt, \tag{10}$$

where $t_p(x)$ is the time when Sb penetrates to depth x and δ is the Dirac delta function, we can then assume that the damage factor f behaves as a step function:

$$f(x,t) = \begin{cases} 0 & t < t_p(x) \\ F(x) & t \geq t_p(x) \end{cases}, \tag{11}$$

where $F(x)$ is a functional form of the damage factor, which accounts for the local Sb concentration at $t \geq t_p$. As observed by Marina et al. [20], the concentration of Sb (c_{Sb}) decreases with increasing depth into the anode support. Based on this observation, we assume a decreasing linear function for $F(x)$ as:

$$F(x) = F_0 - a \times x \tag{12}$$

where F_0 and a are parameters, depending on different operating conditions and Sb concentrations.

To simulate Sb poisoning, the RVE is divided into i layers through the RVE's thickness, which is used to approximate the progression of Sb degradation through the anode's thickness. Degradation is simulated by randomly removing $F(d_i)$ of the Ni elements from each layer, where d_i represents the normalized depth of the ith layer and $F(d_i)$ is the volume fraction of nickel removal at each layer. In this manner, the linear decrease of $F(x)$ is implemented through the anode over a specified degradation time. Fig. 6 illustrates the approximation of the continuous linear function $F(x)$ by the discrete step function $F(d_i)$.

The change in anode performance is evaluated by the normalized electrical conductivity per thickness $\bar{\sigma}^*$ versus the normalized degradation time, t^*, where $\bar{\sigma}^* = \bar{\sigma}_e/\bar{\sigma}^0_e$ and $t^* = t/t^0_p$. t^0_p is the time at which the whole RVE would be poisoned. The electrical conductivity per thickness is normalized by the baseline (no Sb poisoning) ($\bar{\sigma}^0_e$). The damaged electrical conductivity per thickness of the anode ($\bar{\sigma}_e$) is calculated as the average electrical conductivity over the RVE:

$$\bar{\sigma}_e = \frac{D_0 \bar{I}}{L_0 U}, \tag{13}$$

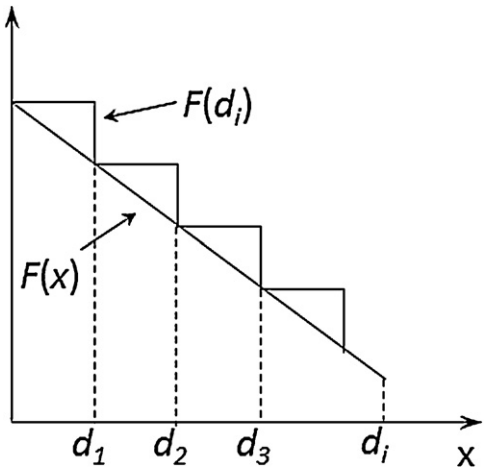

Fig. 6. Schematic illustration of the linear degradation function $F(x)$ and the step approximation $F(d_i)$ used in the FE simulations.

where $\bar{I}$ is the average current and U is the applied voltage. As Ni is removed from the RVE due to Sb poisoning, the effective electrical conductivity of the RVE is degraded due to the poor electrical conductivity of YSZ (Table 3). As Ni is removed, the average current throughout the RVE decreases, causing a decrease in $\bar{\sigma}_e$. As such, the degradation of anode electrical conductivity due to Ni depletion is explicitly resolved in the microstructure-based FE simulations.

To investigate Sb poisoning, six FE simulations were preformed considering the effects of different patterns and magnitudes of Ni depletion in the anode. Three cases were run to investigate the effects of anode thickness (D_o) on Ni depletion, and three cases were run with a linear depletion of Ni with various F_o and a values. For all simulations, the top and bottom sides of the RVE are kept at a constant temperature of 1123 K, and a 1.0 V operating voltage is applied to the anode. Antimony is introduced to the anode with the gas flow at the top surface of the anode ($x = 0$). The material properties of Ni and YSZ used in the FE simulations are listed in Table 3. Note the electrical conductivity of YSZ is assumed to be $^1/_{100}$ of the Ni conductivity. This is done to achieve an initial closed circuit for the current 2-D model. In a more realistic three-dimensional case, the electrical conductivity of YSZ should be even smaller.

Table 3
Baseline material properties of Ni and YSZ.

	Electrical conductivity ($S\,m^{-1}$)	Thermal conductivity (W/(m K))	Specific heat (J/(kg K))
Ni	2.52E+6	90.9	5.4E+2
YSZ	2.52E+4	2	6.3E+2

The first three cases consider the effects of anode thickness (D_o) on the degradation of the anode electrical conductivity due to Sb. The predicted electrical conductivity degradation of Ni–YSZ anodes with different thicknesses is shown in Fig. 7, where a constant $F(d_i)$ is assumed as 0.3. Antimony penetrates the anode at a constant speed, which means $t_p(d_i)$ is proportional to d_i. The thicker anode microstructures are obtained by stitching multiple RVEs together. The results show the different anode thicknesses do not affect the normalized degradation pattern. This indicates that the normalized Sb poisoning pattern is independent of the actual anode thickness, and the 30-μm-thick anode microstructure can be deemed as an RVE. As a result of these calculations, the following analysis was performed on the single RVE (D_0 = 30 μm).

In addition to the overall reduction of electrical conductivity, Ni depletion in the anode also increases current density at localized "hot spots" in the anode as the system attempts to maintain the overall applied voltage (Fig. 8). These current density hot spots will lead to localized temperature increase due to Joule heating (Fig. 9).

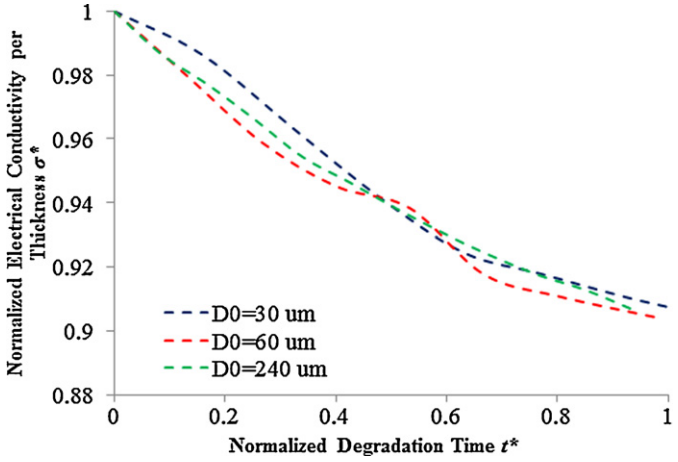

Fig. 7. Plot of the damaged electrical conductivity of the Ni–YSZ anode over time for three different anode thicknesses.

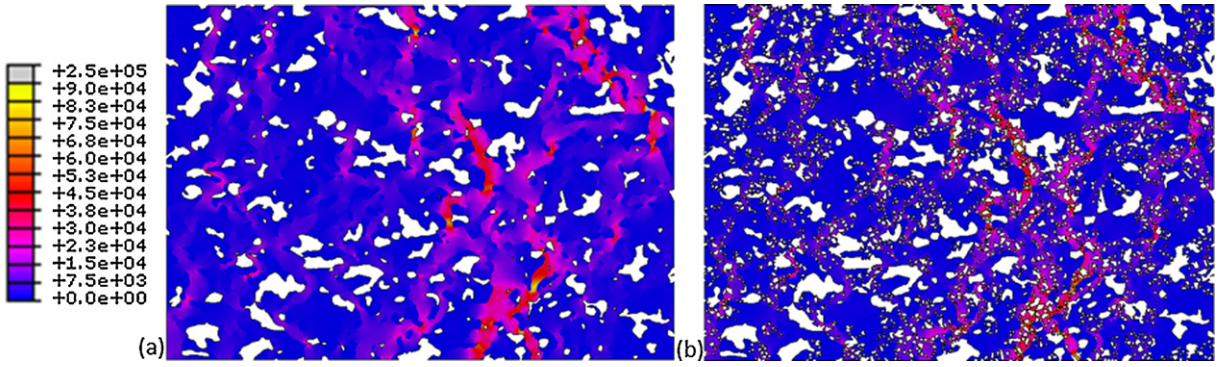

Fig. 8. Distribution of electrical current density (A mm^{-2}) in the Ni–YSZ anode before (a) and after (b) antimony poisoning.

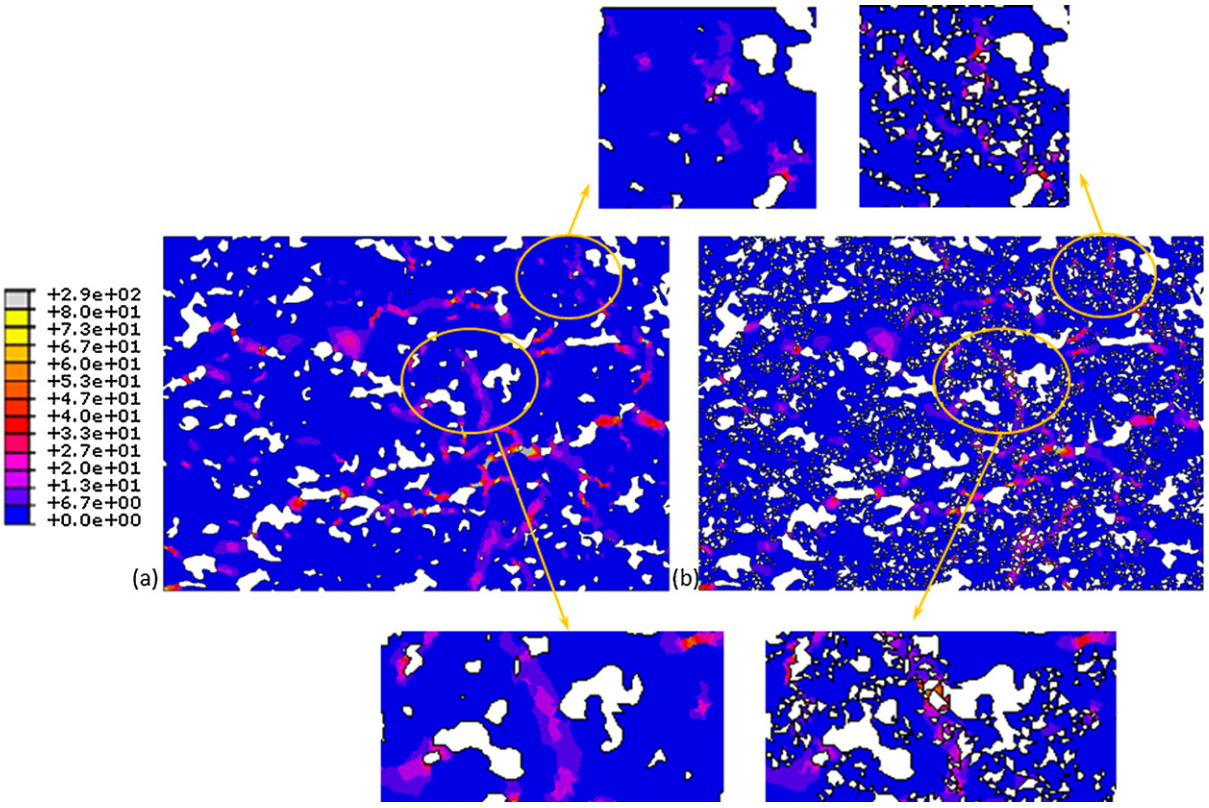

Fig. 9. Distribution of Joule heating in the Ni–YSZ anode before (a) and after (b) antimony poisoning.

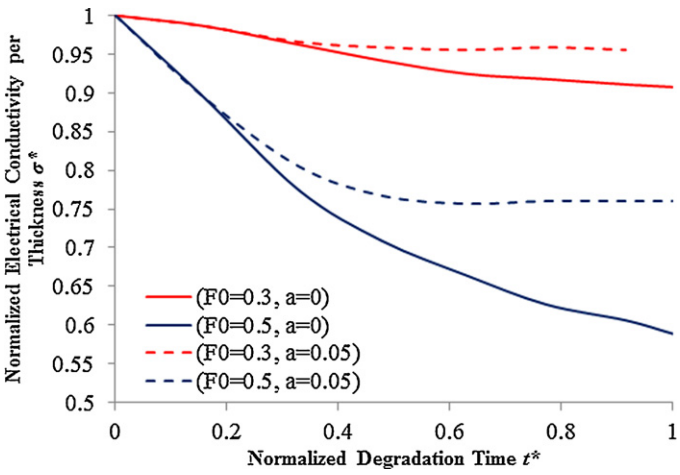

Fig. 10. Plot of the electrical conductivity degradation of the Ni–YSZ anode supports under different environmental Sb concentration conditions.

In the poisoned anode, there are an increased number of hot spots (excessive heating areas) in comparison with the baseline case. This is due to the significant decrease in continuity between the conductive Ni particles after nickel removal, which leads to current density channeling through the remaining Ni particles and increased localized Joule heating near the channels. The localized temperature increase will potentially accelerate secondary reactions and lead to a further reduction in anode performance.

Fig. 10 shows the electrical conductivity of the RVE for four different damage function cases with $F(d_i)$ defined by Eq. (12). These cases are used to represent different operating conditions and Sb concentrations, which can lead to different degradation rates and magnitudes. From the simulations, it is clear the anode generally experiences a rapid initial conductivity drop. Two of the four cases considered in Fig. 10 use a uniform degradation function, where $a = 0$. The other two cases exhibit linearly decreasing degradation along the penetration depth, causing the electrical conductivity to more rapidly reach their respective steady-state plateaus. These results are similar to the experimentally observed effects of Sb poisoning [20]. If $F(d_i)$ is allowed to increase further after $t_p(x)$, it is expected that the Sb poisoning eventually will lead to the ultimate failure of the SOFC.

As a note, the essential purpose of this study is to establish a mechanistic framework to describe the Sb-induced degradation mechanism based on the reconstructed micro-structural model. Though the proposed damage factor may not be precise due to the limited detailed information available for the whole Sb poisoning propagation process, the predicted degradation trend can still be used to establish the maximum permissible percolation loss without affecting the fuel cell performance, which can be further implemented into a stack-level simulation to evaluate the SOFC lifetime.

6. Conclusions

In this paper, we presented a degradation modeling framework for investigating degradation in the electrodes of electrochemical devices such as SOFCs. The modeling framework provides a flexible methodology for investigating various types of degradation in SOFC electrodes. A classification framework was presented that allows the various degradation mechanisms to be categorized based on their electrochemical, structural, and chemical effects on the SOFC. Classifying degradation mechanisms prior to modeling can help identify the appropriate parameters to focus degradation modeling and the proper scales and simulation tools for investigating the problem of interest.

The use of continuum damage mechanics to investigate degradation in SOFC electrodes also was presented. Based on the classification of the degradation mechanism, a damage factor can be used to model the degradation of specific microstructural and electrochemical properties affected by the degradation mechanism of interest. The damage factor model can be coupled to SOFC component, cell, and stack-level models to simulate SOFC performance degradation as was done in Section 5.1 with the H_2S damage model and the cell level DEC model.

The continuum mechanics-based degradation modeling framework has been exercised on two degradation case studies for the SOFC anode: sulfur and antimony poisoning. These two degradation mechanisms have different effects on the SOFC's electrode properties and performance. However, the same modeling strategy was applied to both mechanisms. To model sulfur poisoning, a distributed electrochemistry model [7] was used to investigate the effects of sulfur on the local TPB length and how damage to the local TPB length affects global SOFC performance. The model can incorporate the dependence of sulfur poisoning on the temperature and local concentration of H_2S and could be extended to consider the effects of voltage and SC on poisoning. For antimony poisoning, the effects of Sb on the reduction of normalized electrical conductivity of the anode was predicted with microstructure-based FE methods under different conditions. The results show that with a linearly decreasing damage factor, the correct trend in decreasing anode electrical conductivity can be predicted and matches those observed experimentally for Sb poisoning.

Currently, research into alternative degradation mechanisms in SOFCs and other electrochemical devices is ongoing. We plan to apply the degradation modeling framework to other degradation issues in SOFCs, including those at the stack level. Also, although the framework is discussed in terms of SOFCs, it is applicable to degradation in the electrodes of other electrochemical devices, such as cycling degradation issues found in lithium-ion (Li-ion) and Li–air batteries.

Acknowledgments

The work presented in this paper was funded as part of the Solid-State Energy Conversion Alliance Core Technology Program by the U.S. Department of Energy's National Energy Technology Laboratory. Pacific Northwest National Laboratory is operated for the U.S. Department of Energy by Battelle under contract DE-AC06-76RL01830.

References

[1] M.C. Williams, J.P. Strakey, W.A. Surdoval, Journal of Power Sources 143 (2005) 191–196.
[2] O.A. Marina, C.A. Coyle, E.C. Thomsen, D.J. Edwards, G.W. Coffey, L.R. Pederson, Solid State Ionics 181 (2010) 430–440.
[3] S. Zha, Z. Cheng, M. Liu, Journal of the Electrochemical Society 154 (2007) B201–B206.
[4] T. Cruse, M. Krumpelt, B. Ingram, S. Wang, P.A. Salvador, Ceramic Engineering and Science Proceedings 29 (2009) 147–158.
[5] O.A. Marina, L.R. Pederson, C.A. Coyle, E.C. Thomsen, G.W. Coffey, 11th International Symposium on Solid Oxide Fuel Cells (SOFC-XI)–216th ECS Meeting, Electrochemical Society Inc., Vienna, Austria, 2009, pp. 2125–2130.
[6] M.A. Khaleel, H.M. Zbib, E.A. Nyberg, International Journal of Plasticity 17 (2001) 277–296.
[7] E.M. Ryan, K.P. Recknagle, M.A. Khaleel, Twelfth International Symposium on Solid Oxide Fuel Cells (SOFC-XII), Montrael, CA, 2011.
[8] H. Timmermann, W. Sawady, D. Campbell, A. Weber, R. Reimert, E. Ivers-Tiffee, Journal of the Electrochemical Society 155 (2008) B356–B359.
[9] Y.L. Liu, S. Primdahl, M. Mogensen, Solid State Ionics 161 (2003) 1–10.
[10] C.-K. Lin, T.-T. Chen, Y.-P. Chyou, L.-K. Chiang, Journal of Power Sources 164 (2007) 238–251.
[11] X. Ding, C. Cui, L. Guo, Journal of Alloys and Compounds 481 (2009) 845–850.

[12] J.P. Trembly, R.S. Gemmen, D.J. Bayless, Journal of Power Sources 163 (2007) 986–996.
[13] O.A. Marina, C.A. Coyle, E.C. Thomsen, C.D. Cramer, K.J. Yoon, L.R. Pederson, 34th International Conference and Exposition on Advanced Ceramics and Composites, Daytona Beach, FL, 2010.
[14] O.A. Marina, L.R. Pederson, D.J. Edwards, C.A. Coyle, J.W. Templeton, M.H. Engelhard, Z. Zhu, Solid-State Ionic Devices 5 – 212th Electrochemical Society Meeting, 7–12 October 2007, Electrochemical Society Inc., Washington, DC, United States, 2008, pp. 63–70.
[15] O.A. Marina, L.R. Pederson, E.C. Thomsen, D.J. Edwards, C.A. Coyle, C.N. Cramer, Electrochemical and Solid-State Letters 13 (2010) B63–B67.
[16] J.P. Trembly, R.S. Gemmen, D.J. Bayless, Journal of Power Sources 169 (2007) 347–354.
[17] J.P. Trembly, A.I. Marquez, T.R. Ohrn, D.J. Bayless, Journal of Power Sources 158 (2006) 263–273.
[18] K.C.R. De Silva, B.J. Kaseman, D.J. Bayless, International Journal of Hydrogen Energy 36 (2011) 9945–9955.
[19] W. Liu, X. Sun, L.R. Pederson, O.A. Marina, M.A. Khaleel, Journal of Power Sources 195 (2010) 7140–7145.
[20] O.A. Marina, L.R. Pederson, C.A. Coyle, E.C. Thomsen, P. Nachimuthu, D.J. Edwards, Journal of Power Sources 196 (2011) 4911–4922.
[21] P. Tanasini, M. Cannarozzo, P. Costamagna, A. Faes, J. Van Herle, A. Hessler-Wyser, C. Comninellis, Fuel Cells 9 (2009) 740–752.
[22] H.-Y. Chen, H.-C. Yu, J. Scott Cronin, J.R. Wilson, S.A. Barnett, K. Thornton, Journal of Power Sources 196 (2011) 1333–1337.
[23] O.A. Marina, L.R. Pederson, C.A. Coyle, E.C. Thomsen, D.J. Edwards, Journal of the Electrochemical Society 158 (2011) 36–43.
[24] S.P. Jiang, Y.D. Zhen, Solid State Ionics 179 (2008) 1459–1464.
[25] E.M. Ryan, A.M. Tartakovsky, K.P. Recknagle, C.H. Amon, M.A. Khaleel, Journal of Power Sources 196 (2011) 287–300.
[26] N.M. Galea, J.M.H. Lo, T. Ziegler, Journal of Catalysis 263 (2009) 380–389.
[27] M. Shishkin, T. Ziegler, Journal of Physical Chemistry C 114 (2010) 21411–21416.
[28] K. Lai, B.J. Koeppel, C. Kyoo Sil, K.P. Recknagle, S. Xin, L.A. Chick, V. Korolev, M. Khaleel, Journal of Power Sources 196 (2011) 3204–3222.
[29] FossilEnergy, in: U.S.D.o. Energy (Ed.), Washington, DC, 2011.
[30] L. Yang, Z. Cheng, M. Liu, L. Wilson, Energy and Environmental Science 3 (2010) 1804–1809.
[31] H. Zhu, R.J. Kee, V.M. Janardhanan, O. Deutschmann, D.G. Goodwin, Journal of The Electrochemical Society 152 (2005) A2427–A2440.
[32] Y. Jiang, A.V. Virkar, Journal of the Electrochemical Society 150 (2003) A942–A951.
[33] Z. Cheng, Materials Science, Georgia Institute of Technology, Atlanta, 2008.
[34] T. Yoshizumi, C. Uryu, T. Oshima, Y. Shiratori, K. Ito, K. Sasaki, ECS Transactions 35 (2011) 1717–1725.
[35] R.B. Finkelman, in: M.H. Engel, S.A. Macko (Eds.), Trace and Minor Elements in Coal, Organic Geochemistry, Plenum Press, New York, 1993, pp. 593–607.
[36] S. Dai, R. Zeng, Y. Sun, International Journal of Coal Geology 66 (2006) 217–226.